AMSI VACATIONRESEARCH SCHOLARSHIPS 2020–21

Get a Thirst for Research this Summer

Finding the Body of Minimal Resistance

Juan Sebastian Avila Molina

Supervised by Dr Vera Roshchina

University of New South Wales

February 28, 2021

Vacation Research Scholarships are funded jointly by the Department of Education and the Australian Mathematical Sciences Institute.

AMSI AUSTRALIAN MATHEMATICAL SCIENCES INSTITUTE

Australian Government Department of Education

Abstract

The following report presents the work made on solving Newton's problem of the body of minimum resistance numerically within the standard class of admissible functions (bounded and concave), and defined in a wider range of domains. In this report we provide the techniques utilised in order to formulate and process the optimisation problem, as well as the results obtained. These results suggest that the known feature of a flat region with polygonal shape at the top of the solid of minimal resistance with circular base is also apparent in numerical solutions of regular polygonal base geometry.

Acknowledgements

I wish to express my sincere appreciation to my supervisor Dr Vera Roshchina for her extended guidance during the whole duration of the research project. Dr Roshchina proposed the topic for this project and attentively supervised my work at every stage.

I also want to thank the Australian Mathematics Science Institute for the support offered to undergraduate students like me through programs like the Vacation Research Scholarship. This program made the project feasible to complete within the limited amount of time.

Lastly, I want to thank Dr Édouard Oudet who has made important contributions in recent advancements to Newton's problem of the solid of minimum resistance, and who was kind enough to permit me to use illustrations of his work.

Table of Contents

1 Introduction

As a solid moves through a fluid, a force acting opposite to the direction of motion, commonly known as drag or resistance, is generated due to the difference in velocity between the solid and fluid. One of the first people to study this effect analytically was Isaac Newton, who devised a simple model to describe the fluid dynamics and performed key calculations in which he derived the solid of minimum resistance on a circular base domain using an axial symmetric assumption. Figure 1 below illustrates the main features of Newton's model as described in his 1687 work *"Philosophiæ Naturalis Principia Mathematica"*.

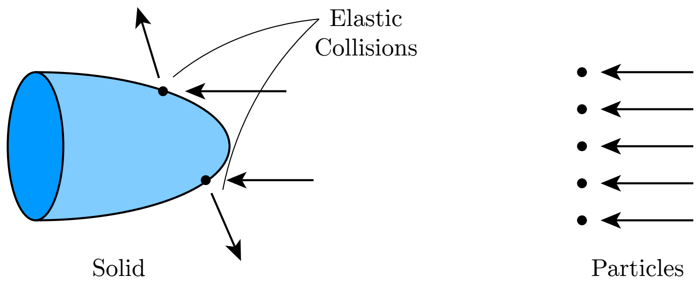

Figure 1: Newton's simplified model of fluid interaction. The fluid consists of 'equal particles freely disposed at equal distances from each other', which do not interact with each other. The resistance effect is modelled by perfect elastic collisions between solid and fluid particles.

While Newton's solid is the true minimiser for all solid of revolutions, a surprising result was found more than 300 years after Newton's original publication which showed that the optimal solid profile that truly minimises the resistance generated across all solids was non-radial and was not unique (Brock et al. 1996). Such discovery prompted a surge of new research which have produced fruitful results in the form of numerical solutions (Buttazzo 2009), however, the problem of finding the minimiser is still open.

The following report presents a professional summary of the research work made on Newton's problem of minimal resistance with emphasis on developing a robust numerical formulation of the original problem, in order to calculate resistances of discretised solids over a flexible range of domains. In this report, the main theory and recent advancements are introduced and serve as the key foundation for the ensuing work. The entire development of the mathematical model is also presented as well as the resistance results obtained numerically over various domain shapes. Furthermore, these results, their value, and the limitations encountered in this project are discussed.

1.1 Statement of Authorship

The work presented was materialised by Mr Avila Molina, as well as the Python code utilised which was written from scratch but which utilised technical modules such as `numpy` and `scipy`. Dr Roshchina supervised the work performed and provided helpful feedback along every stage of the project.

2 Theoretical Background

The main theoretical foundation for the project, and consequently the following report, is Newton's minimum resistance problem. Such can be understood as the problem of finding the solid of minimum resistance in Newton's fluid model. In the modern presentation of the problem (see Appendix A for full derivation), the resistance R can be defined as follows

$$R := \iint_{\Omega} \frac{dxdy}{1 + \|\nabla u(x,y)\|^2}, \tag{1}$$

where the function $u(x,y)$ gives the surface to solid profile on the domain Ω, which in Newton's original problem corresponds to $\Omega = \{(x,y) \in \mathbb{R}^2 : x^2 + y^2 \leq 1\}$.

It is important to note that the resistance of solid can be understood as a *functional* over the domain of admissible functions that generate the solid profile. A functional, in this context, is a mapping from the set of admissible functions u to the real numbers. Newton's problem can then be formulated as the minimisation problem $\min_{u \in \mathcal{U}} R$, where $\mathcal{U}$ is the set of admissible functions. Later, we will present what are the proper characteristics required for a function to be admissible.

The idea of minimising a functional over a set of functions was very new at the time of Newton's publications. Nowadays we classify this class of problems as the subject of 'calculus of variations' which was coined by Euler several decades after Newton's publications (Goldstine 2012).

2.1 Newton's Procedure

While (1) presents a general equation which calculates the resistance of any body with base Ω, Newton used some further simplifications in order to produce his minimal result. The most important was that he assumed the body of minimal resistance must be axially symmetric, or in other words the body profile could be described as $u(x,y) = f(r)$ with $r = \sqrt{x^2 + y^2}$ on $0 \leq r \leq 1$. The equation below presents the simplified resistance expression obtained with this new simplification (refer to Appendix A for derivation).

$$R = \int_0^1 \frac{r\,dr}{1 + \|f'(r)\|^2} \tag{2}$$

Furthermore, some sense of concavity in the profile of the body was assumed by Newton. This generates the admissible set $\mathcal{U} = \{u(x,y) \mid u \text{ is axisymmetric, concave function}\}$ previously introduced in the minimisation problem. Newton used extensive geometric methods in order to find the profile of the minimiser constrained to this admissible set. A thorough description of Newton's work is presented by Chandrasekhar (2003) in his book 'Newton's Principia for the Common Reader', where the original expression for Newton's solution is presented. Such expression is presented in a parametric form and depens on the radius of the circular domain Ω and the maximum height of the solid M. For the standard case where the radius of the base is equal to one, the expression below describes the solution.

$$\begin{aligned} r(t) &= \frac{r_0}{4}\left(t^3 + 2t + \frac{1}{t}\right) \\ u(t) &= M + \frac{r_0}{4}\left(\frac{7}{4} - \frac{3}{4}t^4 - t^2 + \log(t)\right) \end{aligned} \tag{3}$$

with $r_0 \approx 0.351$ and $t \in [1, a]$, $a \approx 1.192$. Figure 2 illustrates Newton's solution for $M = 1$.

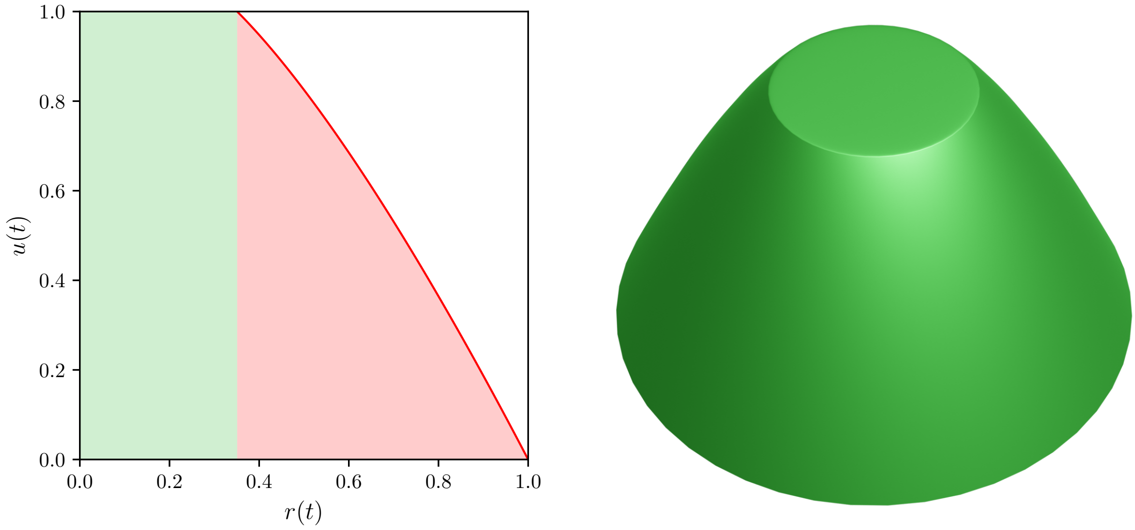

(a) 2D Profile

(b) 3D Render

Figure 2: Newton's solution for $M = R = 1$. a) Green denotes the region where $u(r) = 1$ for $r \in [0, r_0]$. Red denotes the section of the graph given by (3) above. b) Illustration of the solid generated in 3D as profile is revolved around the vertical axis.

An important feature of Newton's solution is the existence a flat region at the top of the solid. We must remember that the problem uses Newton's fluid model with free particles in a rarefied medium instead of the compressible medium which we are accustomed to, hence the results we obtain may not be those we have intuitively thought were best. In fact, we can highlight the fact that relaxing the concavity constraint generates very interesting counter-intuitive results. For instance, consider the following functions:

$$g(r) = 1 - r, \quad 0 \le r \le 1, \qquad \text{and} \qquad h(r) = \begin{cases} r, & 0 \le r < \frac{1}{2} \\ 1 - r, & \frac{1}{2} \le r \le 1 \end{cases}$$

The functions h and g represent concave and non-concave profiles in the domain $r \in [0, 1]$, respectively. Figure 3 presents the solids generated by the functions above. As it is further assumed that the fluid particles vanish as they first interact with the body as the body on the right admits more than one reflection on the convex surface within $0 \le r \le 1/2$, the resistance can be calculated using (2) as well. The resistance for the two objects is calculated to be equal due to the functions h and g having the same gradient square throughout their domain.

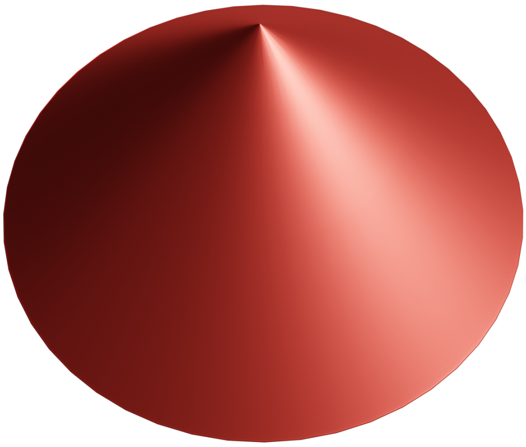

(a) Concave Profile

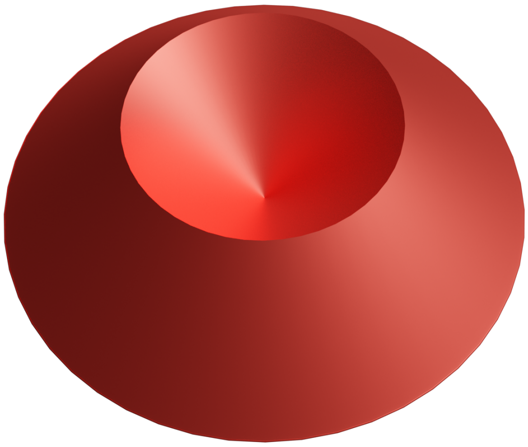

(b) Non-Concave Profile

Figure 3: Solids with equal resistance under Newton's fluid model.

2.2 Non-Axisymmetric Problem

Newton's solution stood uncontested for almost 300 years until Brock et al. (1996) demonstrated that while the solution minimised the resistance over the restricted class of axially symmetric functions, it was not the minimiser for the functional presented in (1) for the set of strictly concave functions. The blunder made by Newton was that he used his intuition to devise his assumptions of axial symmetry and convexity, the latter which we already illustrated interesting results when relaxed. Such oversight demonstrates the importance of rigour in mathematical proofs and hints to a new start from the problem formulation.

It is important to first define a suitable class of admissible functions due to the fact that the resistance equation does not attain a minimiser for the unrestricted set of functions. For this project, we will not consider the case of non-concave bodies, however, recent developments in this area are presented by Mainini et al. (2017) and Comte & Lachand-Robert (2001). Instead, we will use constraints that more accurately represent Newton's imagination. The following constraints are postulated by Buttazzo et al. (1995) and they showed that (1) attains a minimiser within the admissible class that encompass them.

1. Bounded: $0 \leq u(x, y) \leq M$ for all $(x, y) \in \Omega$.
2. Concave: $u(x, y)$ is a concave function in Ω.

To this day, the exact minimiser to (1) on this admissible class has not been found. However, novel research has shown that the solid with minimal resistance attains a flat top of the shape of a polygon. Furthermore the number of sides of such polygon top has been shown experimentally to be a non-increasing function of the maximal solid height M (Lachand-Robert & Peletier 2001). Figure 4 presents some of the most recent computed solutions illustrating the aforementioned features.

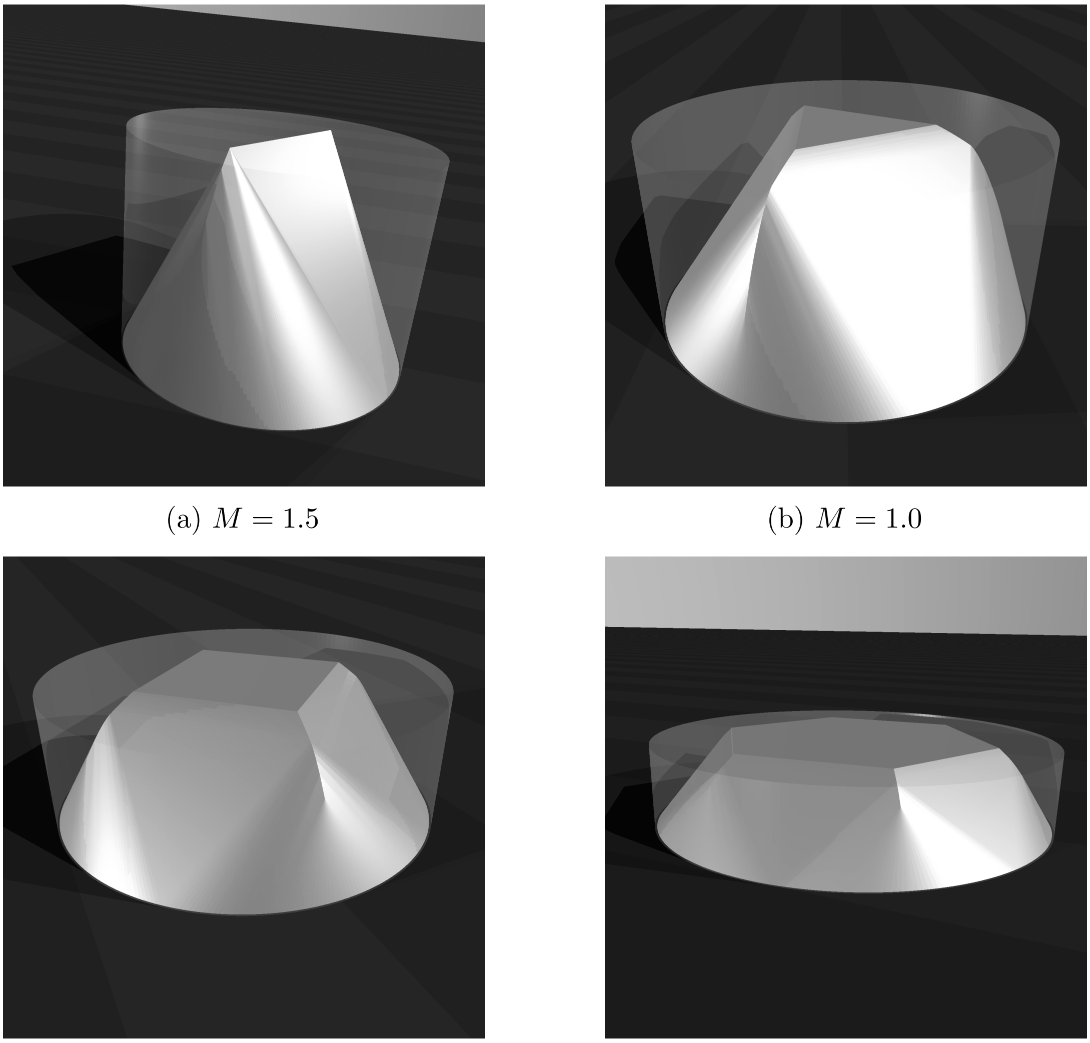

(a) $M = 1.5$ (b) $M = 1.0$ (c) $M = 0.7$ (d) $M = 0.4$

Figure 4: Illustration of numerical solutions found by Lachand-Robert & Oudet (2005) depicting the inverse relationship between number of polygon sides of top face and maximum solid height. Reprinted with permission from Édouard Oudet.

3 Mathematical Model

Having explored the main theoretical background that encompasses Newton's problem, we are now ready to present the problem using the following concise expression:

$$\min_{u(x,y)} \iint_{\Omega} \frac{dxdy}{1 + \|\nabla u(x,y)\|^2} \tag{NP}$$

$$\text{subject to:} \quad u(x,y) \text{ concave;} \quad u(x,y) \in [0, M].$$

It is important to clarify that unlike Newton's simplified expression outlined in (2), the problem above is very hard to tackle analytically. In fact, most of the recent advancements outlined previously used some form of numerical methods in order to process computations.

The scope of this project deals with finding suitable minimisers on various domains, whilst ensuring these results are consistent with known computations. It is hence natural to devise a numerical method that works well for this type of work. Consequently, a suitable modelling technique should satisfy the following points:

- Objective function presented in (NP) can be computed suitably.
- Constraints in (NP) can be implemented based on the model.
- An appropriate optimisation algorithm can be implemented based on the model.
- The model allows for the modification of the domain with ease.

3.1 Potential Modelling Techniques

In the following sections, we will highlight potential ways of solving (NP) as well as provide justifications for the choice of method selected.

3.1.1 Polynomial Approximations

Whilst we know that the function describing the profile of Newton's solid of minimal resistance is non-smooth, the simplicity of these objects means that we can utilise basic analytical tools in order to process the problem. Let $u \in \mathbb{P}(\mathbb{R} \times \mathbb{R})_n$, hence

$$u(x, y) = \sum_{\substack{i+j \leq n \\ i,j \geq 0}} \alpha_{ij} x^i y^j = \sum_{i=0}^{n} \sum_{j=0}^{n-i} \alpha_{ij} x^i y^j, \text{ for some } \alpha_{ij} \in \mathbb{R}.$$

The gradient is computed below which is required to compute the optimal function and may be used in optimisation algorithms.

$$\nabla u = \left[\frac{\partial u}{\partial x}, \frac{\partial u}{\partial y}\right] = \left[\sum_{i=1}^{n} \sum_{j=0}^{n-i} \alpha_{ij} i x^{i-1} y^j, \sum_{i=0}^{n} \sum_{j=1}^{n-i} \alpha_{ij} j x^i y^{j-1}\right]$$

The convexity constraint can be formulated using the fact that when Hu, the Hessian matrix of u, is negative semi-definite it implies that the function is concave.

Sufficient conditions for Hu to be negative semi-definite are $\text{trace}(Hu) < 0$, as well as $\det(Hu) \geq 0$ for all $(x, y) \in \Omega$. Computing these values, we see that we must attain

$$\begin{aligned}
\text{trace}(Hu) &= \frac{\partial^2 u}{\partial x^2} + \frac{\partial^2 u}{\partial y^2} = \sum_{i=2}^{n} \sum_{j=0}^{n-i} \alpha_{ij} i(i-1) x^{i-2} y^j + \sum_{i=0}^{n} \sum_{j=2}^{n-i} \alpha_{ij} j(j-1) x^i y^{j-2} < 0, \\
\det(Hu) &= \frac{\partial^2 u}{\partial x^2} \cdot \frac{\partial^2 u}{\partial y^2} - \left(\frac{\partial^2 u}{\partial x \partial y}\right)^2 \\
&= \left(\sum_{i=2}^{n} \sum_{j=0}^{n-i} \alpha_{ij} i(i-1) x^{i-2} y^j\right) \cdot \left(\sum_{i=0}^{n} \sum_{j=2}^{n-i} \alpha_{ij} j(j-1) x^i y^{j-2}\right) -
\end{aligned}$$

$$\left(\sum_{i=1}^{n}\sum_{j=1}^{n-i}\alpha_{ij}ijx^{i-1}y^{j-1}\right)^2 \geq 0.$$

For a general degree polynomial, the expressions above need to be expanded for closer analysis and thus finding suitable values for α_{ij} become a tedious task which was the main aspect we wanted to avoid using this process. Additionally, the bounding constraint also becomes a similar type of inequality which further adds complexity to the search of suitable parameters. By experimenting with low degree polynomials we may be able to implement the constraints but at the same time, we will obtain non-interesting solids. We hence deem this technique non-suitable for the scope of our project.

3.1.2 Intersection of Half Spaces

Another potential alternative is to model the solids as the intersection of a finite set of half-spaces. It is possible to choose the norms and position vectors that define each half space and so these would become the parameters used to minimise the resistance in the resulting solid. A great advantage of this method is that the concavity constraint is satisfied automatically from the construction. Furthermore, similar techniques were used by Lachand-Robert & Oudet (2005) when generating the computations illustrated in Figure 4, which support the feasibility of such kind of techniques.

However, the computation of the functional does not seem an easy process. In fact, the intersections of the hyperplanes need to be computed in order to find the areas that make up the surface of the body. Furthermore, Lachand-Robert & Oudet (2005) developed a mixed-type algorithm for their optimisation process, as they found classical methods were inadequate for this procedure. Overall we find the implementation of this technique to go beyond the scope of our project, however, it is worth dealing with this technique when refining the solids generated in future work.

3.1.3 Piecewise-Linear Functions

By modelling the 3D surface of the solid as a piecewise-linear function, it is possible to discretise (NP) effectively. Such a procedure would involve the following steps:

1. A lattice of points (x, y) is created within the domain Ω.
2. A triangulation based on the lattice is generated, thus tiling the domain.
3. For every point (x, y), a 'height values' u is chosen such that the solid profile conforms to the boundness and concavity constraints. This is best done by formulating the constraints as linear inequalities, with the process being outlined in later sections.
4. The triples (x, y, u) become points in $\mathbb{R}^3$ and the triangulation scheme allows us to generate the piecewise-linear function from which the gradient can be obtained.
5. The resistance function is then optimised using a sequential least squares programming (SLSQP) algorithm.

Once, a suitable minimiser is found, the solid can then be reconstructed based on the original triangulation as illustrated in Figure 5.

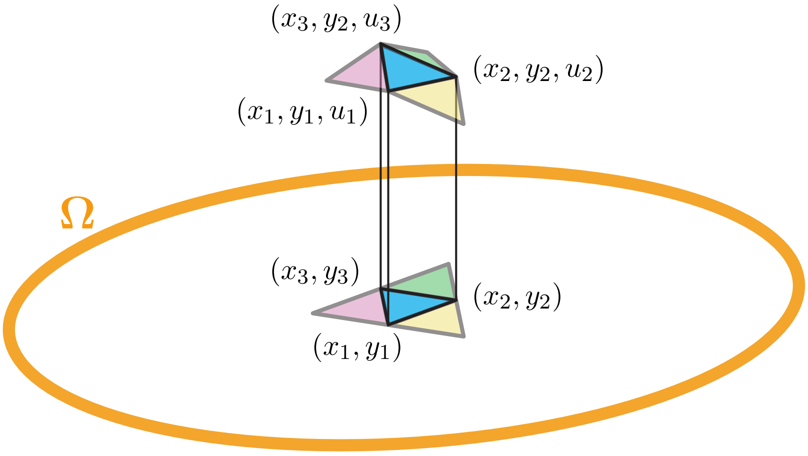

Figure 5: Reconstruction of solid from original triangulation on domain Ω based on piecewise-linear function discretisation.

We think this is a robust method of obtaining minimisers for a wide range of domains as the initial lattice can be generated to any domain with ease, and there are viable methods to tackle all the concerns imposed by the problem. The following section describes the numerical methods used to implement the model suiting (NP) to the scope of our project.

3.2 Discretisation of Newton's Problem

The implementation of the model is done using the programming language Python. In order to obtain a feasible implementation, the process must be able to be computed algorithmically which leads to another layer of mathematical framework to be developed. The complete numerical implementation is hence presented in the following subsections.

3.2.1 Domain

The first thing which must be implemented is a suitable discretisation of the domain which corresponds to the base of the solid. A regular lattice of points is constructed as the basis for the domain as it can be computed orderly and facilitates the process of triangulation. A labelling scheme is proposed where points are indexed by their layer n, section m and value j as $\mathbf{x_{n,m,j}}$.

With the origin set as $\mathbf{x_{0,0,0}}$, the layer of a point indicates the relative position away from the origin. A section refers to their 'angular-position' around the origin starting from region $\pi/2 \leq \theta < 2\pi/3$ and rotating counter-clockwise mapping six regions around the origin. Lastly, the value of a point refers to the relative location the list of points around each section in a counter-clockwise direction.

We denote the set with all possible index within the domain as $\mathcal{P}$. Figure 6a below illustrates a lattice of points with 3 layers ($0 \leq n \leq 2$) and the labelling for each point in the lattice.

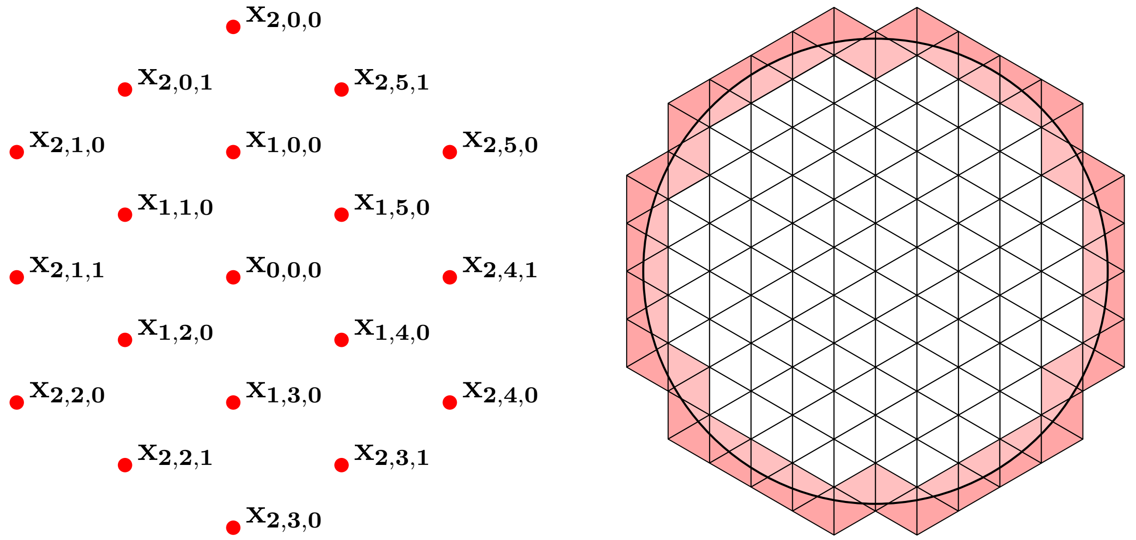

(a) Index scheme of points in regular lattice. (b) Triangulation grid of circular domain.

Figure 6: Illustration of discretisation technique applied to circular domain.

As previously mentioned, a triangulation is used to discretise the space in order to compute the functional numerically. Figure 6b illustrates an undercounting triangulation arrangement of a circular domain with triangles excluded highlighted in red.

Similar to the indexing scheme illustrated in Figure 6a, the triangles are arranged in layers, sections and values in order to ease their management. The notation $\triangle_{n,m,j}$ is used to denote the coordinates of a triangle in layer n, section m and value j. On the first layer ($n = 0$), the triangle in each m-section has coordinates

$$\triangle_{0,m,0} = \left(\mathbf{x_{0,0,0}}, \mathbf{x_{1,m,0}}, \mathbf{x_{1,m+1,0}}\right),$$

where $m \in \mathbb{Z}/6\mathbb{Z}$. For $n \geq 1$ each triangle is constructed recursively as following

$$\triangle_{n,m,j} = \begin{cases} \left(\mathbf{x_{n,m,j/2}}, \mathbf{x_{n,m,j/2+1}}, \mathbf{x_{n-1,m,j/2}}\right), & \text{for } 0 \leq j < 2n-1 \\ & \text{and } j/2 \in \mathbb{Z} \\ \left(\mathbf{x_{n-1,m,(j-1)/2}}, \mathbf{x_{n-1,m,(j+1)/2}}, \mathbf{x_{n,m,(j+1)/2}}\right), & \text{for } 0 \leq j < 2n-1 \\ & \text{and } (j-1)/2 \in \mathbb{Z} \\ \left(\mathbf{x_{n,m,(j+1)/2}}, \mathbf{x_{n-1,m,(j-1)/2}}, \mathbf{x_{n-1,m+1,0}}\right), & \text{for } j = 2n-1 \\ \left(\mathbf{x_{n,m,j/2}}, \mathbf{x_{n,m+1,0}}, \mathbf{x_{n-1,m+1,0}}\right), & \text{for } j = 2n \end{cases}$$

In order to obtain the undercounting tiling of the domain, one must also check that $\|(\triangle_{n,m,j})_k\| \leq 1$, for each coordinate $k \in \{1, 2, 3\}$ in the circular domain case. We then denote the triangulation indexing scheme as $\mathcal{T}$.

On this domain, the function $u(x, y)$ can then be modelled as a piecewise-linear function by stating the function value at each point in the grid and generating the flat faces (plane subsets) from the triangulation obtained. A suitable gradient is then present at each surface which can be used to compute the objective function.

3.2.2 Objective Function

By considering the discretisation of the domain proposed, the continuous functional described in (NP) can be simplified into a discrete form. This can be done by computing this functional for each triangular cell independently and summing the total value over the entire domain.

For each regular triangular cell, the area term $dxdy$ can be expressed as $\sqrt{3}/4s^2$, where s is the side length of each triangle. For a general computation, consider the linear function that describes an arbitrary triangular cell. Hence, let $\ell_{\{a,b,c\}}(x, y) = \alpha x + \beta y + \gamma$ be the linear function such that

$$\ell_{\{a,b,c\}}(x_i, y_i) = u_i, \ \forall i \in \{a, b, c\}, \text{ where } \{a, b, c\} \in \mathcal{T}. \tag{4}$$

The fact that $\{a, b, c\} \in \mathcal{T}$ implies that the points $\mathbf{x}_a, \mathbf{x}_b, \mathbf{x}_c$ define a proper triangular cell within the domain. The condition above generates the following linear system

$$\begin{aligned}
\alpha x_a + \beta y_a + \gamma &= u_a, \\
\alpha x_b + \beta y_b + \gamma &= u_b, \\
\alpha x_c + \beta y_c + \gamma &= u_c.
\end{aligned}$$

Using Cramer's rule, the values for α, β and γ were found algebraically using the `sympy` module as follows.

$$\begin{aligned}
\alpha &= \frac{u_a(y_b - y_c) + u_b(y_c - y_a) + u_c(y_a - y_b)}{x_a y_b - x_a y_c - x_b y_a + x_b y_c + x_c y_a - x_c y_b}, \\
\beta &= \frac{u_a(x_c - x_b) + u_b(x_a - x_c) + u_c(x_b - x_a)}{x_a y_b - x_a y_c - x_b y_a + x_b y_c + x_c y_a - x_c y_b}, \\
\gamma &= \frac{u_a(x_b y_c - x_c y_b) + u_b(x_c y_a - x_a y_c) + u_c(x_a y_b - x_b y_a)}{x_a y_b - x_a y_c - x_b y_a + x_b y_c + x_c y_a - x_c y_b}.
\end{aligned} \tag{5}$$

The gradient of the function is obtained from the expression defined in (4), because at each discretised cell the gradient corresponds to that of the linear function ℓ. Hence

$$\left\|\nabla u(x, y)_{\{a,b,c\}}\right\|^2 = \left\|\nabla \ell_{\{a,b,c\}}(x, y)\right\|^2 = \|[\alpha, \beta]\|^2 = \alpha^2 + \beta^2 \tag{6}$$

Substituting the area term and the discretised version of the gradient shown above, the optimal function can be computed by summing the values from all the triangular cells within the domain. The following discrete sum is obtained for the optimal function by substituting (5) into (6) and then into the resistance functional from (NP).

$$\min_{u_p,\ p \in \mathcal{P}} \frac{\sqrt{3}s^s}{4} \sum_{\{a,b,c\} \in \mathcal{T}} \frac{(x_a y_b - x_a y_c - x_b y_a + x_b y_c + x_c y_a - x_c y_b)^2}{\begin{aligned}&(x_a y_b - x_a y_c - x_b y_a + x_b y_c + x_c y_a - x_c y_b)^2 \\ &+(u_a(y_b - y_c) + u_b(y_c - y_a) + u_c(y_a - y_b))^2 \\ &+ (u_a(x_c - x_b) + u_b(x_a - x_c) + u_c(x_b - x_a))^2\end{aligned}} \tag{O.F.}$$

3.2.3 Constraints

There are only two constraints that need to be considered for the selection of u values. The first and easiest to deal with is $u(x, y) \in [0, M]$ since we can specify that for all $p \in \mathcal{P}$, the discrete values u_p satisfy the condition $0 \leq u_p \leq M$.

The other constraint is that the function $u(x, y)$ must be concave over the domain Ω. This is a bit harder to formulate but the main idea is constraining all discrete u_p values to be 'below' each affine plane that defines a triangulation cell at the surface level of u. In mathematical terms, we want $u_q \leq \ell_{\{a,b,c\}}(x_j, y_j)$ for all $j \in \mathcal{P}$ and for all $\{a, b, c\} \in \mathcal{T}$.

Whilst this algorithm will work, it is very inefficient and has a memory complexity of $|\mathcal{T}|^{|\mathcal{P}|}$ which grows very rapidly as the discretisation is refined. We can instead use the fact that convexity is a local property and thus check the condition above for a neighbourhood of each triangulation cell. Figure 7 below illustrates two possible neighbourhoods that can serve for this application with the points in red being checked against the plane spanning the triangulation cell shown as the shaded triangle.

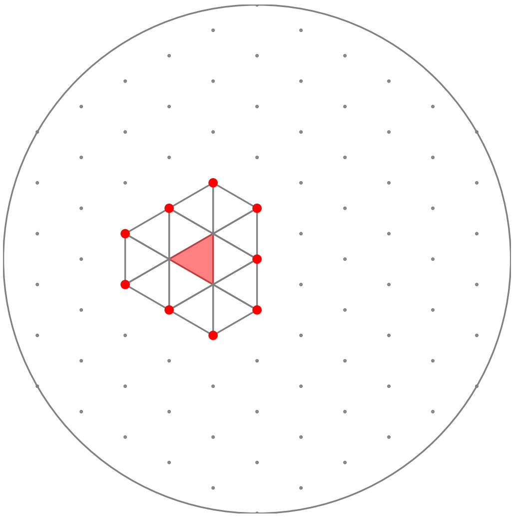

(a) Nine Neighbouring Check

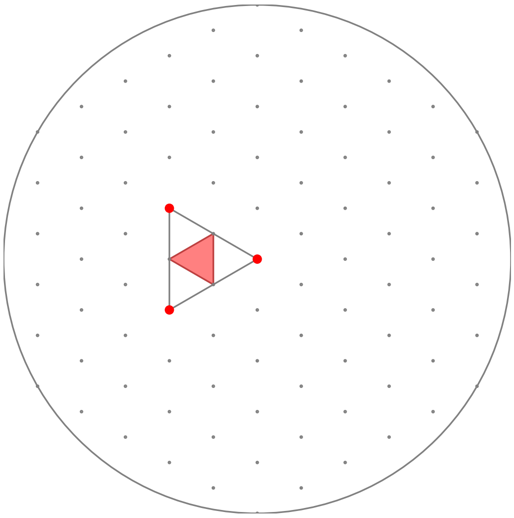

(b) Three Neighbouring Check

Figure 7: Neighbouring checks used for discretised concavity constraints at local regions. The 'nine neighbouring check' offers a more consistent way of ensuring concavity in rough areas such as the boundary of the domain, however, the 'three neighbouring check' works well in smooth surfaces and runs faster.

With this change, the memory complexity is in the order of $|T|$ thus illustrating a great improvement over the naive method. Letting $\mathcal{N}_{\{a,b,c\}} \subseteq \mathcal{P}$ be the set of points in the neighbourhood of the triangle cell indexed by $\{a, b, c\} \in \mathcal{T}$, the concavity constraint can then be formulated as follows

$$u_j \leq \frac{\begin{array}{l}(u_a(y_b - y_c) + u_b(y_c - y_a) + u_c(y_a - y_b))\, x_j \\ \quad + (u_a(x_c - x_b) + u_b(x_a - x_c) + u_c(x_b - x_a))\, y_j \\ \qquad + (u_a(x_b y_c - x_c y_b) + u_b(x_c y_a - x_a y_c) + u_c(x_a y_b - x_b y_a))\end{array}}{x_a y_b - x_a y_c - x_b y_a + x_b y_c + x_c y_a - x_c y_b}, \forall \{a, b, c\} \in \mathcal{T},\ \forall j \in \mathcal{N}_{\{a,b,c\}}.$$

3.2.4 Optimisation Algorithm

In order to minimise the discretised function, a suitable optimisation algorithm must be devised or chosen from available modules. The minimisation problem studied can be characterised as a constrained minimisation problem of multivariate scalar functions and as such a SLSQP algorithm will be utilised as it is suitable for these type of problems.

The gradient of the objective function (O.F.) is required in order to use this algorithm. This can be found by considering each point and each triangular cell containing such point and computing the gradient contribution. The expression for the gradient is presented below and while it looks cumbersome, it is rather easy to code with a single loop.

$$\nabla \text{O.F.} = \frac{\sqrt{3}s^s}{4}\left[\cdots,\ \underbrace{-2\sum_{\{a,b,c\}\in\mathcal{T}} \frac{\begin{gathered}(x_ay_b - x_ay_c - x_by_a + x_by_c + x_cy_a - x_cy_b)^2\\ \cdot\left[(y_b - y_c)(u_a(y_b - y_c) + u_b(y_c - y_a) + u_c(y_a - y_b))\right.\\ \left.+\ (x_c - x_b)(u_a(x_c - x_b) + u_b(x_a - x_c) + u_c(x_b - x_a))\right]\end{gathered}}{\begin{gathered}\left[(x_ay_b - x_ay_c - x_by_a + x_by_c + x_cy_a - x_cy_b)^2\right.\\ +(u_a(y_b - y_c) + u_b(y_c - y_a) + u_c(y_a - y_b))^2\\ \left.+\ (u_a(x_c - x_b) + u_b(x_a - x_c) + u_c(x_b - x_a))^2\right]^2\end{gathered}}}_{a\text{th term}},\cdots\right]^T$$

A trust-region constrained algorithm can also be utilised, however, it yields slower results than the SLSQP algorithm and requires computing the Hessian matrix of (O.F.).

4 Results

Having implemented all the mathematical machinery required in order to find numerical minimisers of the resistance function for varying domain geometry, a neatly written Python script was produced. When running the program, the only parameter that was varied was the spacing between the points in the lattice s. We note a technical lower bound of was 0.1 as memory limits were experienced by the compiler when running a more refined mesh. The maximal height and area (A) of each domain were fixed to 1 and π, respectively, thus preserving the $M : A$ ratio which allows the comparison between different domain geometries linearly. Table 1 below presents the results obtained.

Table 1: Summary of results obtained with domains with $A = \pi$, $M = 1$, and $s = 0.1$.

Domain	Area Utilised	Resistance	Resistance Per Area Utilised
Circle	2.8752 (91.5%)	1.0450	0.3635
Square	2.8579 (91.0%)	1.0307	0.3606
Triangle	2.4942 (79.4%)	1.2971	0.5201

Figure 8, Figure 9 and Figure 10 on the following page illustrate the triangulation grid and minimiser obtained for the circular, square and triangular domains, respectively.

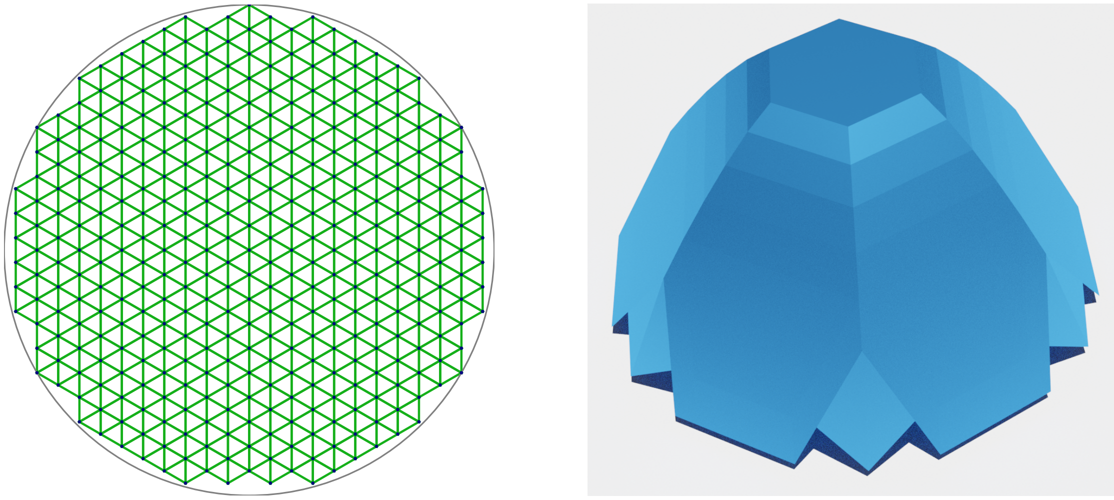

(a) Triangulation Grid (b) Optimal Solid

Figure 8: Solid of Minimal Resistance With Circular Domain

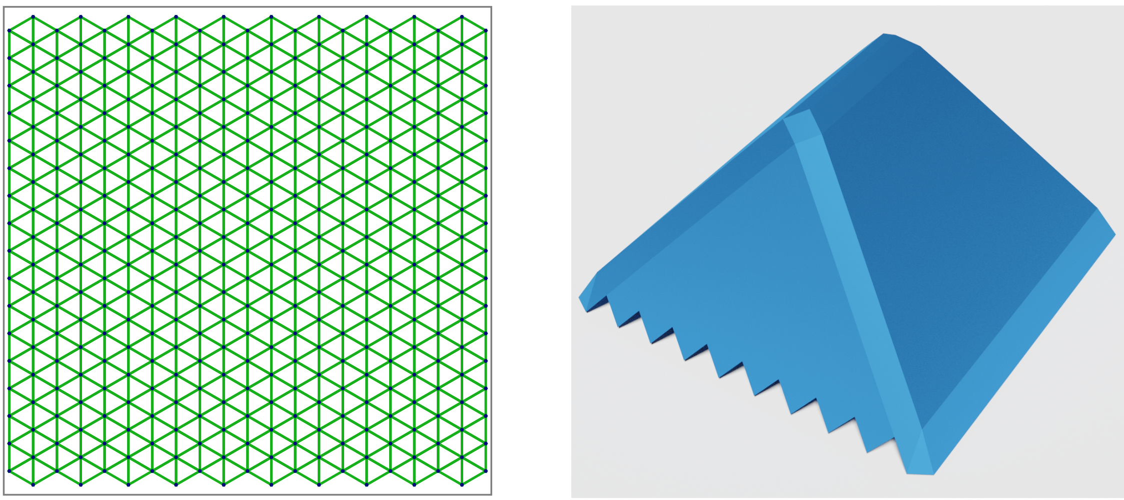

(a) Triangulation Grid (b) Optimal Solid

Figure 9: Solid of Minimal Resistance With Square Domain

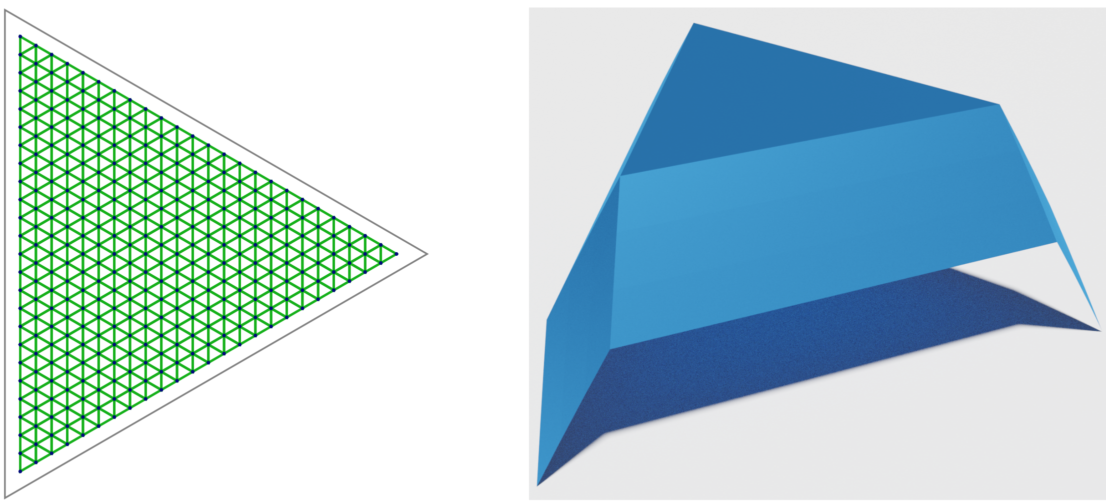

(a) Triangulation Grid (b) Optimal Solid

Figure 10: Solid of Minimal Resistance With Triangular Domain

5 Discussion and Conclusion

The results obtained illustrate that minimisers for the square and triangular domain exhibit similar behaviour to those observed in circular studies, such as those obtained by Lachand-Robert & Oudet illustrated in Figure 4, namely a flat top with polygonal shape. Furthermore, the quantitative results shown in Table 1 demonstrate that the resistance per area utilised, which was calculated in order to account for the gaps in the domain and the discretised mesh, varied significantly based on the geometry of the domain. The minimiser obtained in the triangular and square domains had resistance values 43.1% higher and 0.8% lower than the resistance obtained for the circular domain, respectively.

In order to corroborate the results obtained, we show that the quantitative resistance results obtained are comparable to those found in previous numerical experiments. Due to the fact that the results for minimisers in non-circular domains are the first of its kind, we can only check the circular results obtained. Table 2 presents a comparison of the results obtained in this project with Newton's solution and the best known minimisers.

Table 2: Comparison of resistance values obtained with known results in circular domains.

Result*	Resistance Per Area Utilised	Improvement Over Newton's Solution
Solution Illustrated in Figure 8	0.3635	3.014%
Newton's Solution†	0.3748	–
Best Known Solid†	0.3622	3.362%

* With $M = 1$ for all solids compared.
† Results obtained from Lachand-Robert & Oudet (2005).

Nevertheless, it is important to recognise some limitations encountered by the modelling process and the results obtained. While the resistance per area served as a suitable way of accounting for the undercounting method of tiling a domain, it may generate misleading results as the actual domain calculated had non-regular geometries. This is combined with the fact that the most refined mesh that could be analysed was still very coarse with an edge size of 0.1, thus further accentuating the non-regularity of the domains. Lastly, we must highlight that there is potential bias in the results introduced from the geometry of the mesh, hence while the results obtained may be the best according to our mesh, it is likely these are not the most optimal.

Using a more powerful computer will allow us to further refine the mesh obtained and obtain more accurate results, however, the bias of the selected mesh will still be apparent if the same regular lattice is used. Introducing local mesh refinements will be beneficial in reducing the number of constraints required as only local sections of the surface are changed per iteration of the minimisation algorithm, and in reducing bias as the mesh geometry will be altered, however, a more complex model will have to be devised. In spite of these limitations, we can conclude that the model utilised was adequate for the the scope of the project and the aims presented in the proposal were achieved successfully.

References

Brock, F., Ferone, V. & Kawohl, B. (1996), 'A symmetry problem in the calculus of variations', *Calculus of Variations and Partial Differential Equations* **4**(6), 593–599.

Buttazzo, G. (2009), A survey on the Newton problem of optimal profiles, *in* 'Variational Analysis and Aerospace Engineering', Springer New York, New York, NY, pp. 33–48.

Buttazzo, G., Ferone, V. & Kawohl, B. (1995), 'Minimum Problems over Sets of Concave Functions and Related Questions', *Mathematische Nachrichten* **173**(1), 71–89.

Chandrasekhar, S. (2003), *Newton's Principia for the Common Reader*, Clarendon Press, pp. 593–599.

Comte, M. & Lachand-Robert, T. (2001), 'Newton's problem of the body of minimal resistance under a single-impact assumption', *Calculus of Variations and Partial Differential Equations* **12**, 173–211.

Goldstine, H. (2012), *A History of the Calculus of Variations from the 17th through the 19th Century*, Studies in the History of Mathematics and Physical Sciences, Springer New York.

Lachand-Robert, T. & Oudet, E. (2005), 'Minimizing within Convex Bodies Using a Convex Hull Method', *SIAM Journal on Optimization* **16**.

Lachand-Robert, T. & Peletier, M. (2001), 'Newton's Problem of the Body of Minimal Resistance in the Class of Convex Developable Functions', *Mathematische Nachrichten* **226**(1), 153–176.

Mainini, E., Monteverde, M., Oudet, E. & Percivale, D. (2017), 'Newton's aerodynamic for non-convex bodies', *Rendiconti Lincei - Matematica e Applicazioni* **28**, 885–896.

Newton, I. (1687), *Philosophiæ Naturalis Principia Mathematica*, Royal Society.

Plakhov, A. & Aleksenko, A. (2010), 'The problem of the body of revolution of minimal resistance', *ESAIM: Control, Optimisation and Calculus of Variations* **16**(1), 206–220.

Appendices

A Derivation of Resistance Equations

The following derivations are adapted from work by Plakhov & Aleksenko (2010).

Consider an orthogonal space with a flow of particles moving vertically downwards parallel to the z-axis with velocity $\mathbf{w} = (0, 0, -1)$. A compact set $B \subset \mathbb{R}^3$ with base $\Omega = \{(x, y) \in \mathbb{R}^2 : x^2 + y^2 \leq 1\}$ is generated with the upper part of the boundary ∂B given by a function $u(x, y)$.

Suppose a single flow particle makes contact with points in the boundary ∂B finitely many times and then moves freely afterwards. By Newton's model, these interactions are equivalent to elastic collisions and the trajectories can be modelled as reflections on the tangent to the surface. Let $\mathbf{v}$ denote the particle's final velocity with $\mathbf{v} = (0, 0, -1)$ if there are no reflections.

Each particle that collides with the body B transmits its momentum equal to the particle mass times the change in velocity $\mathbf{v} - \mathbf{w} = (v_x, v_y, v_z) - (0, 0, -1) = (v_x, v_y, v_z + 1)$.

Summing all the momenta over the domain Ω, the resistance of the body is then equal to $-\rho\mathbf{R}(B)$, where

$$\mathbf{R}(B) = \iint_{\Omega} (v_x, v_y, v_z + 1)\, dx\, dy, \tag{7}$$

and ρ is the flow density. However, Newton's problem only deals with the resistance parallel to the direction of particle flow, hence the desired value R corresponds only to the third component of $\mathbf{R}(B)$.

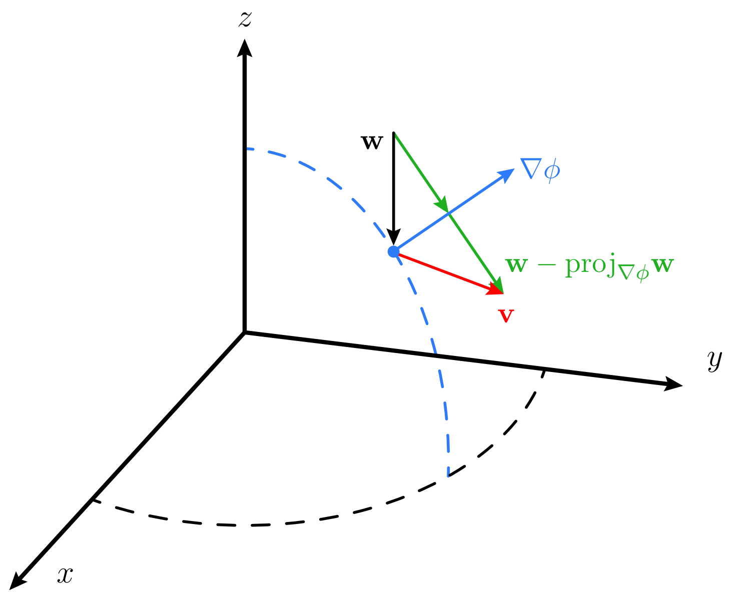

Figure 11: Illustrative diagram of particle/solid momentum exchange.

With reference to Figure 11, the velocity $\mathbf{v}$ can be computed using the gradient vector of the surface $\phi(x,y,z) = u(x,y) - z$ which corresponds to the normal direction of the tangent plane at the point $(x, y, u(x, y))$. Computing the gradient of this function, we obtain

$$\nabla\phi = (\partial_x\phi, \partial_y\phi, \partial_z\phi) = (\partial_x u, \partial_y u, -1)$$

Using basic vector geometry, we can then compute the final velocity as follows

$$\begin{aligned}
\mathbf{v} &= 2(\mathbf{w} - \mathrm{proj}_{\nabla\phi}\mathbf{w}) - \mathbf{w} = \mathbf{w} - 2\mathrm{proj}_{\nabla\phi}\mathbf{w} \\
\mathbf{v} &= (0,0,-1) - 2\,\frac{\nabla\phi\cdot(0,0,-1)}{\|\nabla\phi\|^2}\nabla\phi \\
&= (0,0,-1) - 2\,\frac{(\partial_x u, \partial_y u, -1)\cdot(0,0,-1)}{\|(\partial_x u, \partial_y u, -1)\|^2}\,(\partial_x u, \partial_y u, -1) \\
&= (0,0,-1) - \frac{2}{\partial_x u^2 + \partial_y u^2 + 1}\,(\partial_x u, \partial_y u, -1) \\
&= \left(-\frac{2\partial_x u}{1+\|\nabla u\|^2}, -\frac{2\partial_y u}{1+\|\nabla u\|^2}, \frac{1-\|\nabla u\|^2}{1+\|\nabla u\|^2}\right).
\end{aligned}$$

Using the velocity and the third component of (7), the resistance value parallel to the direction of particle flow is calculated to be

$$\begin{aligned}
R = \iint_\Omega v_z + 1\; dx\,dy &= \iint_\Omega \left(\frac{1-\|\nabla u\|^2}{1+\|\nabla u\|^2} + 1\right) dx\,dy \\
&= 2\iint_\Omega \frac{dx\,dy}{1+\|\nabla u\|^2}\;.
\end{aligned}$$

For axisymmetric bodies where the profile can be substituted as $u(x,y) = f(\sqrt{x^2+y^2})$, we can use polar coordinates substitution, namely $r = \sqrt{x^2+y^2}$ over the domain $0 \le r \le 1$ and $0 \le \theta \le 2\pi$ (equivalent to Ω), in order to simplify the integral. Using the standard substitutions on the resistance integral we work as follows

$$\begin{aligned}
R &= 2\iint_\Omega \frac{dx\,dy}{1+\|\nabla u\|^2} \\
&= 2\int_0^1\int_0^{2\pi} \frac{r\,d\theta\,dr}{1+\|f'(r)\|^2} \\
&= 4\pi\int_0^1 \frac{r\,dr}{1+\|f'(r)\|^2}
\end{aligned}$$

These integrals are equivalent to those presented in (1), only differing by a constant factor which is done to simplify the expression and does not affect the minimisation procedure.